J. Fluid Mech. (2001), *vol.* 433, *pp.* 135–160. Printed in the United Kingdom

Bending and stretching of thin viscous sheets

By N. M. RIBE

Institut de Physique du Globe, 4 place Jussieu, 75252 Paris cédex 05, France
e-mail: ribe@ipgp.jussieu.fr

(Received 16 November 1999 and in revised form 18 October 2000)

Thin viscous sheets occur frequently in situations ranging from polymer processing to global plate tectonics. Asympotic expansions in the sheet's dimensionless 'slenderness' $\epsilon \ll 1$ are used to derive two coupled equations that describe the deformation of a two-dimensional inertialess sheet with constant viscosity μ and variable thickness and curvature in response to arbitrary loading. Three model problems illustrate the partitioning of thin-sheet deformation between stretching and bending modes: (i) A sheet with fixed (hinged or clamped) ends, initially flat and of length L_0 and thickness $H_0 \equiv \epsilon L_0$, inflated by a constant excess pressure ΔP applied to one side ('film blowing'). The sheet deforms initially by bending on a time scale $\mu\epsilon^4/\Delta P \equiv \tau_b$, and thereafter by stretching except in bending boundary layers of width $\delta \sim L_0(t/\tau_b)^{-1/3}$ at the clamped ends. (ii) An initially horizontal 'viscous beam' with length L_0 and thickness $H_0 \equiv \epsilon L_0$, clamped at one end, deforms by bending on a time scale $\tau_b = \mu H_0^2/g\delta\rho L_0^3$ until it hangs nearly vertically. Thereafter it deforms by bending in a thin boundary layer at the clamped end, and elsewhere by stretching on a slow time scale $\epsilon^{-2}\tau_b$. (iii) A sheet extruded horizontally at speed U_0 from a slit of width H_0 in a gravitational field deforms primarily by bending on a time scale $(\mu H_0^2/U_0^3 g\delta\rho)^{1/4}$. The sheet's 'hinge point' moves in the direction opposite to the extrusion velocity, which may explain the observed retrograde motion of subducting oceanic lithosphere ('trench rollback').

1. Introduction

Thin deformable viscous sheets occur frequently in both engineering and geophysics. A principal goal of polymer and glass processing is to produce thin fluid layers which stiffen upon cooling to become bottles, tubes, or flat sheets. On volcanic islands such as Hawaii, thin stiff sheets with characteristic thickness ~ 1 cm and lateral dimension ~ 100 m form whenever the surface of a hot body of lava is cooled by exposure to the air. Such sheets encase slowly moving 'pahoehoe' lava flows, and cover the surfaces of fresh Hawaiian lava lakes in a network of deformable plates interacting along their common boundaries. The same dynamics occurs on the scale of the Earth, whose mechanically strong outer shell (the lithosphere) is an assemblage of thin mutually interacting sheets with characteristic thickness ~ 100 km and lateral dimension ~ 1000–$10\,000$ km.

All the systems just mentioned display highly complex rheological behaviour that typically involves memory, temperature-dependence, and nonlinearity. The study of idealized thin-sheet models with Newtonian viscous rheology nonetheless remains a necessary first step. Such models were first developed for applications in the glass and polymer industries. Pearson & Petrie (1970*a*, *b*) derived equations for steady flow in an axisymmetric tubular film inflated by an applied excess pressure and deforming by stretching alone ('film blowing'). The many subsequent extensions and

refinements of this model were summarized by Fliert, Howell & Ockendon (1995), who themselves derived general equations for unsteady blowing of films with arbitrary shape. Buckmaster, Nachman & Ting (1975) extended the thin-sheet model to include deformation by bending as well as stretching, and studied the behaviour of a viscous sheet ('viscida') whose ends are moved together (or apart) with a specified velocity. Howell (1996) re-examined this model, determining the time scales involved and considering the effects of inertia.

In geophysics, thin viscous sheet models have been widely used to model the long-term and large-scale deformation of continents. The approach was pioneered by England & McKenzie (1982, 1983), who derived equations for the flow in a thin flat sheet of fluid having a power-law rheology. A more recent application of a similar model is Ellis, Fullsack & Beaumont (1995), who give a comparative summary of previous work. Applications of thin-sheet models to global-scale plate tectonics include Ribe (1992) and Weinstein & Olson (1992). A more general theory including bending (but without curvature effects) was derived by Medvedev & Podladchikov (1999).

Much insight into the behaviour of viscous sheets can be gained from the well-developed linear theory of elastic shells (e.g. Novozhilov 1959; Goldenveizer 1961; Calladine 1983; Niordson 1985; Ciarlet 1998). In the incompressible limit (Poisson's ratio $= 1/2$), the equations of linear (small strain) elastostatics become identical to those of slow viscous flow if displacements are interpreted as velocities and the shear modulus as viscosity. Results from elastic shell theory can therefore be 'recycled' directly for application to viscous flow. The most common approach to elastic shell theory is to reduce the three-dimensional equations of elastostatics to two-dimensional equations for the displacements of the shell's 'midsurface', defined such that any normal drawn to it intersects the shell's outer surfaces at equal distances. The core of the theory is a set of expressions relating bending moments and stress resultants (integrals of stress across the shell) to the kinematic quantities (extensions, shear, curvature changes, and twist) that describe the deformation of the midsurface. The derivation of these expressions is in most cases based on the so-called Kirchhoff hypotheses that linear elements normal to the undeformed midsurface remain straight, become normal to the deformed midsurface, and suffer no extension. The classic derivation of shell theory along these lines is that of Love (1944), who treated the general case of an arbitrary doubly curved sheet deformed by both stretching and bending. Love's theory neglects the 'mixed' terms that represent the coupling between bending and stretching that inevitably arises when a shell is curved. Despite many subsequent attempts to remedy this omission, there remains considerable disagreement about the proper form of these terms (see, e.g. Niordson 1985). An alternative approach to shell theory is the use of asymptotic expansions to effect systematic reductions of the full three-dimensional equations of elastostatics without invoking the Kirchhoff hypotheses (e.g. Goldenveizer 1963; Sanchez-Palencia 1990; Green & Zerna 1992; Ciarlet 1998). However, this approach has been applied primarily to special cases, and has not yet led to a uniformly valid theory for shells of arbitrary shape subjected to arbitrary loading.

The incomplete state of elastic shell theory means that its results cannot simply be borrowed without further ado. I therefore proceed from first principles, deriving a set of uniformly valid equations for the deformation of two-dimensional thin viscous sheets of arbitrary shape under arbitrary loading. The limitation to two dimensions is deliberate: such sheets display rich dynamics that must be understood before more general three-dimensional sheets are considered, and are moreover excellent models

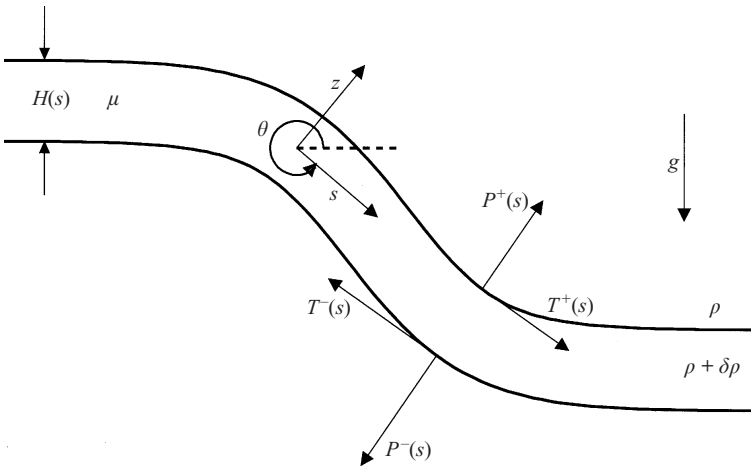

FIGURE 1. Definition sketch of the model. A two-dimensional viscous sheet has constant viscosity μ, constant excess density $\delta\rho$, and variable thickness $H(s)$, where s is the arclength along the sheet's midsurface $z = 0$. The midsurface has inclination $\theta(s)$ from the horizontal and curvature $K(s) = \mathrm{d}\theta/\mathrm{d}s$. The velocities in the s- and z-directions are $u(s, z)$ and $w(s, z)$, respectively, and the velocities at the midsurface are $u(s, 0) \equiv u_0(s)$ and $w(s, 0) \equiv w_0(s)$. Creeping (inertialess) flow in the sheet is driven both by its buoyancy and by externally applied normal stresses $P^{\pm}(s)$ and tangential stresses $T^{\pm}(s)$ that vary over a characteristic distance L. Arrows show the sense of positive $P^{\pm}(s)$ and $T^{\pm}(s)$.

for a variety of quasi-two-dimensional processes from polymer film manufacture to subduction. The derivation presented here has three essential features: a complete scaling analysis, which reveals the leading-order scales of the velocities and stresses; systematic reduction of the full governing equations using asymptotic expansions based on the scaling; and a careful evaluation of the error of the final approximate theory, using analytical solutions of the exact equations for viscous flow. While the 'thin-sheet equations' that result agree in many respects with those obtained by previous authors, they also contain new terms that improve the theory's accuracy. I will discuss numerical solutions of the thin-sheet equations for three model problems: a sheet inflated by an excess pressure applied to one side ('film blowing'); a clamped 'viscous beam' deforming under its own weight; and a dense sheet extruded horizontally in a gravitational field.

2. Exact model equations and boundary conditions

Figure 1 shows a definition sketch of the model. A two-dimensional viscous sheet has constant viscosity μ, constant excess density $\delta\rho$ relative to an ambient fluid, and a variable thickness $H(s)$, where s is the arclength along the sheet's midsurface $z = 0$. Let

$$H(s) = H_0 f(s),$$

where H_0 is a characteristic value of the sheet's thickness and $f(s)$ is a dimensionless function of order unity. The midsurface is inclined at an angle $\theta(s)$ from the horizontal, and its curvature $K(s) = \mathrm{d}\theta/\mathrm{d}s$ is positive when the centre of curvature is in the $+z$-direction. The velocities in the s- and z-directions are $u(s, z)$ and $w(s, z)$, respectively, and the velocities at the midsurface are $u(s, 0) \equiv u_0(s)$ and $w(s, 0) \equiv w_0(s)$. Flow in the sheet is driven both by its buoyancy and by externally applied normal stresses $P^{\pm}(s)$ and tangential stresses $T^{\pm}(s)$ that vary over a characteristic lateral length scale L.

The equations governing creeping (inertialess) flow in the sheet are

$$\frac{\partial u}{\partial s} + \frac{\partial}{\partial z}(hw) = 0, \tag{2.1a}$$

$$\frac{\partial \sigma_{ss}}{\partial s} + \frac{\partial}{\partial z}(h\sigma_{zs}) + \sigma_{zs}\frac{\partial h}{\partial z} = -hg_s\delta\rho, \tag{2.1b}$$

$$\frac{\partial}{\partial z}(h\sigma_{zz}) + \frac{\partial \sigma_{zs}}{\partial s} - \sigma_{ss}\frac{\partial h}{\partial z} = -hg_z\delta\rho, \tag{2.1c}$$

where σ_{ij} is the stress tensor,

$$h = 1 - zK,$$

$$g_s\boldsymbol{s} + g_z\boldsymbol{z} \equiv -g(\boldsymbol{s}\sin\theta + \boldsymbol{z}\cos\theta)$$

is the gravitational acceleration vector, and $\boldsymbol{s}$ and $\boldsymbol{z}$ are unit vectors in the s- and z-directions.

The components of the stress tensor are related to the velocity components by

$$\sigma_{ss} = -p + \frac{2\mu}{h}\left(\frac{\partial u}{\partial s} - Kw\right), \quad \sigma_{zz} = -p + 2\mu\frac{\partial w}{\partial z},$$

$$\sigma_{zs} = \mu\left[\frac{1}{h}\frac{\partial w}{\partial s} + h\frac{\partial}{\partial z}\left(\frac{u}{h}\right)\right].$$

2.1. *Global force and torque balance*

Equations for the global force balance are obtained by integrating the momentum equations (2.1b) and (2.1c) across the sheet, yielding

$$\frac{\mathrm{d}N}{\mathrm{d}s} - KQ = -Hg_s\delta\rho - F_s^+ - F_s^-, \tag{2.2a}$$

$$\frac{\mathrm{d}Q}{\mathrm{d}s} + KN = -Hg_z\delta\rho - F_z^+ - F_z^-, \tag{2.2b}$$

where

$$N = \int_{-H/2}^{H/2}\sigma_{ss}\,\mathrm{d}z, \quad Q = \int_{-H/2}^{H/2}\sigma_{zs}\,\mathrm{d}z$$

are the 'resultants' of the fibre stress σ_{ss} and the shear stress σ_{zs}, respectively,

$$F_j^\pm = \pm h_\pm\left(\sigma_{zj}^\pm - \sigma_{sj}^\pm\tan\alpha_\pm\right), \tag{2.3}$$

$\sigma_{ij}^\pm$ are the stresses at the sheet's surfaces $z = \pm H(s)/2$, $h_\pm = 1 \mp HK/2$, and

$$\alpha_\pm = \pm\tan^{-1}\left(\frac{1}{2h_\pm}\frac{\mathrm{d}H}{\mathrm{d}s}\right)$$

are the inclinations of the sheet's outer surfaces relative to the midsurface. The quantities $F_j^\pm$ are the forces acting in the j (= z or s) direction on the sheet's outer surfaces, but measured per unit area of the midsurface.

The equation for global torque balance is obtained by multiplying (2.1b) by z and then integrating, yielding

$$\frac{\mathrm{d}M}{\mathrm{d}s} - Q = \tfrac{1}{12}KH^3g_s\delta\rho - \tfrac{1}{2}H(F_s^+ - F_s^-), \tag{2.4}$$

where

$$M = \int_{-H/2}^{H/2} z\sigma_{ss}\,\mathrm{d}z$$

is the first moment of the fibre stress ('bending moment'). Because N is the 'zeroth' moment of $\sigma_{ss}(z)$, I shall henceforth call it the 'stretching moment' to emphasize its analogy with M. Elimination of Q from (2.2) and (2.4) now yields

$$\frac{\mathrm{d}^2M}{\mathrm{d}s^2} + KN = -Hg_z\delta\rho + \frac{\delta\rho}{12}\frac{\mathrm{d}}{\mathrm{d}s}(KH^3g_s) - F_z^+ - F_z^- - \frac{1}{2}\frac{\mathrm{d}}{\mathrm{d}s}[H(F_s^+ - F_s^-)], \tag{2.5a}$$

$$\frac{\mathrm{d}N}{\mathrm{d}s} - K\frac{\mathrm{d}M}{\mathrm{d}s} = -Hg_s\delta\rho\left(1 + \frac{K^2H^2}{12}\right) - F_s^+ - F_s^- + \tfrac{1}{2}HK(F_s^+ - F_s^-). \tag{2.5b}$$

2.2. *Boundary conditions*

Continuity of normal and tangential stress at the boundaries of the sheet requires

$$\sigma_{zz}^{\pm}\cos^2\alpha_{\pm} - \sigma_{zs}^{\pm}\sin 2\alpha_{\pm} + \sigma_{ss}^{\pm}\sin^2\alpha_{\pm} = P^{\pm}, \tag{2.6a}$$

$$\sigma_{zs}^{\pm}\cos 2\alpha_{\pm} + \tfrac{1}{2}(\sigma_{zz}^{\pm} - \sigma_{ss}^{\pm})\sin 2\alpha_{\pm} = T^{\pm}, \tag{2.6b}$$

where $P^{\pm}$ and $T^{\pm}$ are the normal and tangential stresses exerted by the external fluid on the sheet's outer surfaces. By solving (2.6) for $\sigma_{zz}^{\pm}$ and $\sigma_{zs}^{\pm}$ and substituting the results into (2.3), one obtains

$$F_z^{\pm} = \pm h_{\pm}(P^{\pm} + T^{\pm}\tan\alpha_{\pm}), \tag{2.7a}$$

$$F_s^{\pm} = \pm h_{\pm}(T^{\pm} - P^{\pm}\tan\alpha_{\pm}). \tag{2.7b}$$

3. Scaling analysis

All the above equations are exact. I now exploit the slenderness of the sheet to derive a simpler set of 'thin sheet' equations that are valid when

$$\epsilon \equiv H_0/L \ll 1,$$

where L is the characteristic length scale over which the flow varies along the sheet. The second dimensionless parameter in the problem is the curvature

$$\kappa \equiv KL,$$

which unlike ϵ may attain values of order unity. The above definitions imply that L is the smallest lateral length scale, i.e. the smaller of the radius of curvature K^{-1} and the characteristic wavelength of the applied loading.

The first step in the derivation is a scaling analysis to determine how the velocities and stresses scale as functions of ϵ and κ. I begin by breaking down the flow within the sheet into simple components. The analytical solutions for a loaded annulus to be discussed below show that in the limit $\epsilon \ll 1$, the velocity components, pressure, and fibre stress have the forms

$$u = \sum_{n=0} u_n\zeta^n, \quad w = \sum_{n=0} w_n\zeta^n, \quad p = \sum_{n=0} p_n\zeta^n, \quad \sigma_{ss} = \sum_{n=0}(\sigma_{ss})_n\zeta^n, \tag{3.1}$$

where $\zeta = z/H_0$. Thus u_0 is the part of the lateral velocity that is constant across the sheet; u_1 is the part that varies linearly across the sheet; and so on. Define also

$$\omega = \frac{\mathrm{d}w_0}{\mathrm{d}s} + Ku_0, \quad \Omega = -\frac{\mathrm{d}\omega}{\mathrm{d}s}, \quad \Delta = \frac{\mathrm{d}u_0}{\mathrm{d}s} - Kw_0,$$

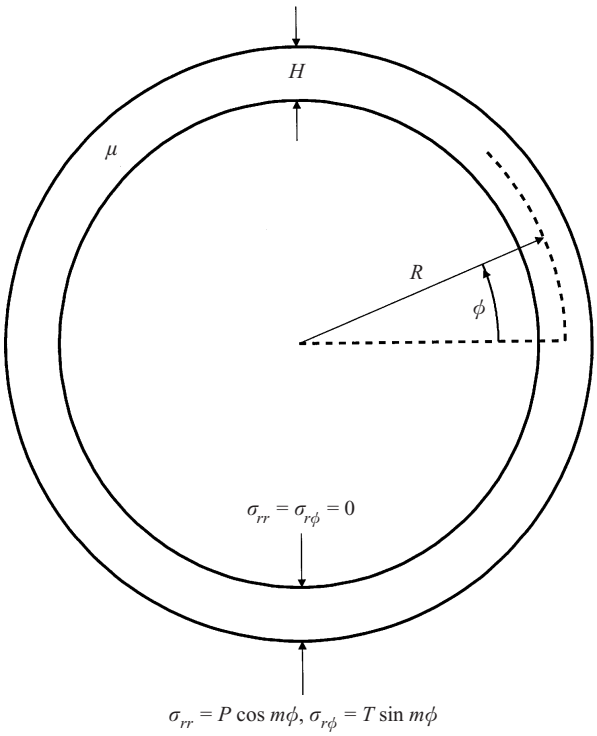

FIGURE 2. Model problem for scaling analysis and evaluation of the accuracy of the thin-sheet equations. A cylindrical annulus with mean radius R, thickness H, and viscosity μ is deformed by a normal stress $\sigma_{rr} = P\cos m\phi$ and a tangential stress $\sigma_{r\phi} = T\sin m\phi$ applied to its outer surface $r = R + H/2$. The sheet's inner surface is stress-free.

which are respectively the rates of rotation, bending, and stretching of the material surface that coincides instantaneously with the midsurface. A related quantity appearing frequently in the theory of elastic shells (*modulo* a time derivative) is $\Omega + K\Delta$, the rate of change of the curvature of the coincident material surface (e.g. Novozhilov 1959, p. 25).

The expansions (3.1) imply nothing about how u_n, w_n, p_n, and $(\sigma_{ss})_n$ scale as functions of ϵ and κ. This scaling turns out to be quite complicated; the surest way to get it right is to solve analytically a simple model problem. The one I shall use (figure 2) is that of a cylindrical annulus with mean radius R, thickness H, and viscosity μ, deformed by a normal stress $\sigma_{rr} = P\cos m\phi$ and a tangential stress $\sigma_{rs} = T\sin m\phi$ applied to its outer surface $r = R + H/2$. The sheet's inner surface is stress-free. For this problem, $s = R\phi$, $L = R/m$, $\epsilon = H/L$, and $\kappa = m^{-1}$. The full range of dimensionless curvature can thus be attained simply by varying m, the limit $m \to \infty$ corresponding to a flat sheet.

Two cases must be distinguished: harmonic loading ($m > 0$), and isotropic loading ($m = 0$).

3.1. *Harmonic loading* ($m > 0$)

The flow for this case was determined by solving the biharmonic equation for the streamfunction in cylindrical coordinates. The resulting scales, determined by expanding the variables in powers of ζ and ϵ, are as follows, where [ ] denotes the

maximum of the enclosed quantities:

$$\frac{\epsilon^2\mu}{L}u_1 \sim \frac{\epsilon^3\mu}{L}w_0 \sim \epsilon^2 p_1 \sim \epsilon^2(\sigma_{ss})_1 \sim \epsilon^3\mu\omega \sim \frac{M}{L^2} \sim [P, T[\kappa, \epsilon]],$$

$$u_0 \sim \frac{L}{\epsilon^3\mu}[P[\kappa, \epsilon^3], T[\kappa^2, \epsilon^2]],$$

$$\frac{\mu}{L}w_1 \sim \epsilon p_0 \sim \epsilon\mu\Delta \sim [P[\kappa, \epsilon], T],$$

$$(\sigma_{ss})_0 \sim \frac{1}{\epsilon}[P\epsilon^2[\kappa, \epsilon], T],$$

$$N \sim L[P[\kappa, \epsilon^5], T].$$

Expressions for u_0, w_0, N and M, expanded in powers of ϵ for arbitary $m > 1$, are given in the Appendix for both normal and tangential loading.

Three implications of the above scales should be noted. First, for all values of κ, the dominant component of u, w, p and σ_{ss} is either the constant ($n = 0$) or the linear ($n = 1$) term. The quadratic and higher terms ($n \geqslant 2$) are smaller by factors of at least ϵ^2 (for u and w) or ϵ (for p and σ_{ss}). Second, $w_1 \leqslant \epsilon^2 w_0$ for all κ. This is consistent with the Kirchhoff assumption that lines normal to the midsurface undergo negligible extension. Third, the relative magnitudes of the $n = 0$ and $n = 1$ components of u, p and σ_{ss} depend on whether the sheet's curvature is 'high' ($\kappa \gg \epsilon$) or 'low' ($\kappa \sim \epsilon$). At high curvature, $u_0 \gg u_1$; but the two are of the same order at low curvature. For normal loading, the 'bending stresses' p_1 and $(\sigma_{ss})_1$ always dominate the 'stretching stresses' p_0 and $(\sigma_{ss})_0$, regardless of the curvature. For tangential loading, the bending stresses dominate the stretching stresses only at high curvature; at low curvature, the two are of the same order. In no case do the stretching stresses greatly exceed the bending stresses.

The only scales required for the asymptotic expansions below are those for u, w, and p. The leading-order scale for each of these variables is just the larger of the scales for the constant ($n = 0$) and linear ($n = 1$) terms, or

$$u \sim \frac{L}{\epsilon^3\mu}[P[\kappa, \epsilon], T[\kappa^2, \epsilon^2]], \quad \frac{\epsilon^3\mu}{L}w \sim \epsilon^2 p \sim [P, T[\kappa, \epsilon]]. \tag{3.2}$$

3.2. *Isotropic normal loading ($m = 0$)*

For isotropic ($m = 0$) normal loading, the Stokes equations have the exact solution

$$u = 0, \quad w = \frac{PR^2(1 - \epsilon^2/4)^2}{4\mu\epsilon r}, \quad p = -\frac{P(1 + \epsilon/2)^2}{2\epsilon}, \tag{3.3}$$

where $\epsilon = H/R$. The only lateral length scale is the cylinder radius R, which I shall henceforth denote by L to facilitate comparison with the case $m > 0$. The scales implied by (3.3) are

$$\frac{\epsilon\mu}{L}w_0 \sim \frac{\mu}{L}w_1 \sim \epsilon p_0 \sim \epsilon(\sigma_{ss})_0 \sim (\sigma_{ss})_1 \sim \epsilon\mu\Delta \sim \frac{N}{L} \sim \frac{M}{\epsilon^2 L^2} \sim P. \tag{3.4}$$

For this simple isotropic model, the tangential velocity $u \equiv 0$ by symmetry. However, u will generally be non-zero in more realistic situations involving sheets that are not complete cylinders. If the sheet's radius of curvature is of the same order as its length, the continuity equation then implies $u \sim w$. Combining this result with (3.4) yields

the scaling for a deformation dominated by stretching:

$$u \sim w \sim \frac{PL}{\epsilon\mu}, \quad p \sim \frac{P}{\epsilon}. \tag{3.5}$$

These scales are identical to those used by Fliert *et al.* (1995).

4. Thin-sheet equations

I shall now use asymptotic expansions in the small parameter ϵ to express the moments N and M in terms of the velocities u_0 and w_0 at the midsurface.

4.1. *Asymptotic expansions*

The leading-order terms in the asymptotic expansions are those revealed by the scaling analysis of the preceding section. Consider first bending-dominated deformations in the high-curvature limit $\kappa = O(1)$, for which the scales (3.2) are

$$u \sim w \sim \frac{SL}{\mu\epsilon^3}, \quad p \sim \frac{S}{\epsilon^2}, \tag{4.1}$$

where $S = P$ for normal loading or T for tangential loading. Curvatures $\kappa = O(\epsilon)$ or smaller need not be considered, as the resulting expressions for N and M are merely (low-curvature) limiting forms of the expressions for $\kappa = O(1)$.

In view of (3.1) and (4.1), the appropriate expansions for bending-dominated deformation are

$$\{u, w\} = \frac{SL}{\mu\epsilon^3}\sum_{m=0}\sum_{n=0}\epsilon^m\zeta^n\{u_{mn}(\xi), w_{mn}(\xi)\}, \quad p = \frac{S}{\epsilon^2}\sum_{m=0}\sum_{n=0}\epsilon^m\zeta^n p_{mn}(\xi), \tag{4.2}$$

where $\xi = s/L$. Moreover,

$$h = 1 - \epsilon\kappa(\xi)\zeta, \tag{4.3}$$

where $\kappa = LK(s)$. Note that the variables u, w, and p are dimensional, whereas ξ, ζ, κ, u_{mn}, w_{mn}, and p_{mn} are dimensionless.

Now substitute the expansions (4.2) and (4.3) into the governing equations (2.1*a*) and the boundary conditions (2.6), assuming that $\alpha_\pm \sim \mathrm{d}H/\mathrm{d}s = O(\epsilon)$ (larger values of $\mathrm{d}H/\mathrm{d}s$ would be incompatible with the thin-sheet approximation). By setting to zero separately the coefficients of each term $\epsilon^m\zeta^n$ in each equation, one obtains a set of coupled linear equations for u_{mn}, w_{mn}, and p_{mn}. To simplify the notation, let

$$\omega_m = w'_{m0} + \kappa u_{m0}, \quad \Omega_m = -\omega'_m, \quad \Delta_m = u'_{m0} - \kappa w_{m0},$$

where primes denote differentiation with respect to ξ. The quantities ω_m, Ω_m, and Δ_m are the parts proportional to ϵ^{m-3} of the rotation, bending, and stretching rates of the material surface that coincides instantaneously with the midsurface.

One need determine only those coefficients u_{mn}, w_{mn}, and p_{mn} that contribute to N and M. The two-term expansions for the latter are

$$N = -\frac{LSf}{12}\{12p_{10} + f^2p_{12} - 24\Delta_2 + 2\kappa f^2(w_{22} - u'_{11}) + \epsilon[12p_{20} + f^2p_{22} - 24\Delta_3 + 2\kappa f^2(w_{32} - u'_{21})] + O(\epsilon^2)\}, \tag{4.4a}$$

$$M = -\frac{L^2Sf^3}{12}[p_{01} - 2u'_{11} + \epsilon(p_{11} - 2u'_{21}) + O(\epsilon^2)], \tag{4.4b}$$

where coefficients that later prove to be identically zero have been omitted. In particular, I have anticipated the results

$$\Delta_0 = \Delta_1 = 0, \tag{4.5}$$

which show that the sheet is inextensible to order ϵ^2.

The solution procedure described above now yields

$$u_{11} = -\omega_0, \quad u_{21} = -\omega_1, \quad w_{22} = -\Omega_0/2, \quad w_{32} = -\Omega_1/2, \tag{4.6a}$$

$$p_{01} = -2\Omega_0, \quad p_{11} = -2\Omega_1, \quad p_{12} = -\kappa\Omega_0, \quad p_{22} = -\kappa\Omega_1, \tag{4.6b}$$

$$p_{10} = -\tfrac{1}{2}\kappa f^2\Omega_0 - 2\Delta_2, \quad p_{20} = -\tfrac{1}{2}\kappa f^2\Omega_1 - 2\Delta_3 - \tfrac{1}{2}(\hat{P}^+ + \hat{P}^-), \tag{4.6c}$$

where $\hat{P}^\pm = P^\pm/S$. Note that to determine p_{20} one must apply the boundary conditions on the normal stress at $\zeta = \pm f/2$. Now (4.2) and (4.5) imply

$$\Omega = \frac{S}{\epsilon^3\mu L}[\Omega_0 + \epsilon\Omega_1 + O(\epsilon^2)], \quad \Delta = \frac{S}{\epsilon\mu}[\Delta_2 + \epsilon\Delta_3 + O(\epsilon^2)]. \tag{4.7}$$

Upon substituting (4.6) into (4.4) and rewriting the results using (4.7), one obtains

$$N = 4\mu H\Delta + \tfrac{5}{6}\mu H^3 K\Omega + \tfrac{1}{2}H(P^+ + P^-), \tag{4.8a}$$

$$M = \tfrac{1}{3}\mu H^3\Omega. \tag{4.8b}$$

The three terms in (4.8*a*) require some comment. The most important are the first two, both of which appear at lowest order in the expansion (4.4*a*) and are independent of the boundary conditions. The first term is independent of the curvature K, and represents the sheet's resistance to stretching. The quantity 4μ that appears there is often called the sheet's 'Trouton viscosity' (Howell 1996). The second term is the integrated excess tension that arises when a curved sheet is bent. When a flat sheet is bent, the stress σ_{ss} is proportional to z to lowest order, so that its integral across the sheet is zero. Finite curvature breaks this symmetry: $|\sigma_{ss}|$ is now larger on the side of the midsurface that is towards the centre of curvature. Consequently, σ_{ss} contains a part that varies quadratically with z, which when integrated across the sheet gives the second term in (4.8*a*). The third term appears only at order ϵ, through the coefficient p_{20} in (4.4*a*). It represents the additional integrated tension generated by a net compressional ($P^+ + P^- < 0$) or extensional ($P^+ + P^- > 0$) stress applied normal to the sheet's midsurface, and vanishes if the loading is purely tangential.

Consider now stretching-dominated deformations, for which the appropriate scales are (3.5). Upon carrying out asymptotic expansions similar to those described above, one finds the following expressions for the moments N and M:

$$N = 4\mu H\Delta + \tfrac{1}{2}H(P^+ + P^-), \tag{4.9a}$$

$$M = \frac{\mu H^3}{3}(\Omega + K\Delta) + \frac{H^3}{8}\frac{\mathrm{d}}{\mathrm{d}s}(T^+ + T^-) - \tfrac{1}{2}H^3 g_z\delta\rho. \tag{4.9b}$$

Because stretching now dominates over bending, the expression (4.9*a*) for N lacks the term proportional to Ω ($= 5\mu H^3 K\Omega/6$) that appears in (4.8*a*). For the same reason, the expression (4.9*b*) for M contains a new term proportional to Δ ($= \mu H^3 K\Delta/3$) which represents the bending moment induced by the stretching of a curved sheet. The last two terms in (4.9*b*) involve the applied loads $T^\pm$ and $g_z\delta\rho$, and appear only at second order in the asymptotic expansion.

4.2. *Composite expressions*

Composite expressions for N and M valid for both bending and stretching are now obtained by adding (4.8) and (4.9) and then subtracting the terms common to both, yielding

$$N = 4\mu H\Delta + \tfrac{5}{6}\mu H^3 K\Omega + \tfrac{1}{2}H(P^+ + P^-), \tag{4.10a}$$

$$M = \frac{\mu H^3}{3}(\Omega + K\Delta) + \frac{H^3}{8}\frac{\mathrm{d}}{\mathrm{d}s}(T^+ + T^-) - \tfrac{1}{2}H^3 g_z \delta\rho. \tag{4.10b}$$

Direct testing against the analytical solutions for a loaded annulus shows that (4.10) are valid to within a uniform relative error of order ϵ^2 for either normal or tangential loading and for either high ($\kappa \sim 1$) or low ($\kappa \sim \epsilon$) curvature. The composite expansions fail only for normal loading of a nearly flat sheet ($\kappa \ll \epsilon$), in which case N is poorly predicted by (4.10*a*). The reason is that $N \sim PL[\kappa, \epsilon^5]$ is very small when $\kappa \ll \epsilon$, and can only be determined using a higher-order asymptotic expansion. However, this failure is of no consequence, because the stretching of a normally loaded flat sheet is negligible relative to its bending.

4.3. *Thin-sheet equations*

The thin-sheet equations are obtained by substituting (2.7) and (4.10) into (2.5) and neglecting small terms. Among the terms thus eliminated are the small corrections to the buoyancy terms and several small terms involving $P^\pm$ and $T^\pm$. Also eliminated are the terms arising from the stretching-induced contribution $\mu H^3 K\Delta/3$ to the bending moment (4.10*b*), which are smaller (by factors of ϵ^2 and K^2H^2) than the corresponding terms due to the stretching moment $N = 4\mu H\Delta$. The equations thus obtained are

$$\frac{\mu}{3}\left[\frac{\mathrm{d}^2}{\mathrm{d}s^2} + \tfrac{5}{2}K^2\right](H^3\Omega) + 4\mu K H\Delta = Hg\delta\rho\cos\theta - P^+ + P^- - \left(\frac{\mathrm{d}H}{\mathrm{d}s} + \frac{H}{2}\frac{\mathrm{d}}{\mathrm{d}s}\right)(T^+ + T^-), \tag{4.11a}$$

$$\frac{\mu}{2}\left[K\frac{\mathrm{d}}{\mathrm{d}s} + \frac{5}{3}\frac{\mathrm{d}K}{\mathrm{d}s}\right](H^3\Omega) + 4\mu\frac{\mathrm{d}}{\mathrm{d}s}(H\Delta) = Hg\delta\rho\sin\theta - T^+ + T^- - \frac{H}{2}\frac{\mathrm{d}}{\mathrm{d}s}(P^+ + P^-). \tag{4.11b}$$

These equations involve no assumption regarding the relative magnitudes of $P^\pm$ and $T^\pm$.

5. Comparative accuracy

I now evaluate the accuracy of the thin-sheet equations (4.11) in comparison with previously published theories. I begin by rewriting the equations in the forms

$$\mu\left[\frac{1}{3}\frac{\mathrm{d}^2}{\mathrm{d}s^2} + \lambda_1 K^2\right](H^3\Omega) + 4\mu K H\Delta = Hg\delta\rho\cos\theta - P^+ + P^- - \lambda_2\left(\frac{\mathrm{d}H}{\mathrm{d}s} + \frac{H}{2}\frac{\mathrm{d}}{\mathrm{d}s}\right)(T^+ + T^-), \tag{5.1a}$$

					Relative error			
					$\kappa = O(1)$		$\kappa = O(\epsilon)$	
Theory	Loading	λ_1	λ_2	λ_3	u_0, w_0, Ω	Δ	u_0, w_0, Ω	Δ
1	P	5/6	—	1	ϵ^2	ϵ^2	ϵ^2	ϵ^2
	T	5/6	1	—	ϵ	ϵ	ϵ^2	ϵ^2
2	P	5/6	—	0	ϵ	ϵ	ϵ^2	1
	T	5/6	0	—	ϵ	ϵ	1	ϵ^2
3	P	0	—	1	ϵ^2	1	ϵ^2	1
	T	0	1	—	ϵ	1	ϵ^2	ϵ^2
4	P	0	—	0	ϵ	1	ϵ^2	1
	T	0	0	—	ϵ	1	1	ϵ^2
	$P(m=0)$	—	—	—	ϵ^2	ϵ^2	—	—

TABLE 1. Relative errors for loaded annulus model.

$$\mu\left[\left(\lambda_1 - \frac{1}{3}\right)K\frac{\mathrm{d}}{\mathrm{d}s} + \lambda_1\frac{\mathrm{d}K}{\mathrm{d}s}\right](H^3\Omega) + 4\mu\frac{\mathrm{d}}{\mathrm{d}s}(H\Delta)$$
$$= Hg\delta\rho\sin\theta - T^+ + T^- - \lambda_3\frac{H}{2}\frac{\mathrm{d}}{\mathrm{d}s}(P^+ + P^-), \qquad (5.1b)$$

where λ_1, λ_2 and λ_3 are variable 'switch' parameters. The various published thin-sheet theories correspond to different values of λ_1, the coefficient of the bending-induced stretching moment in (4.10*a*), and the coefficients λ_2 and λ_3 of the non-local inhomogeneous terms that involve lateral derivatives of the load distribution.

The accuracy of a given theory can be measured by comparing its predictions with the analytical solutions for the loaded annulus model of figure 2. Table 1 shows the relative errors in the bending rate Ω and the stretching rate Δ predicted by several theories. The errors are shown for harmonic ($m > 0$) and isotropic ($m = 0$) loading, normal (P) and tangential (T) loading, and high ($\kappa = O(1)$) and low ($\kappa = O(\epsilon)$) curvature. In all cases, the relative errors of the velocity components u_0 and w_0 are of the same order in ϵ as the errors of Ω.

Theory 1 is the one derived in this paper. It is the most accurate of those considered, with all relative errors vanishing in the limit $\epsilon \to 0$. Theory 2 shows that neglecting the non-local loading terms ($\lambda_2 = \lambda_3 = 0$) degrades the accuracy of the solutions overall and generates errors of order unity at low curvature. Theory 3 shows that the stretching rate is poorly predicted (except for tangential loading at low curvature) if the bending contribution to N is neglected ($\lambda_1 = 0$). Theory 4 corresponds to the incompressible and two-dimensional limits of the theory of Timoshenko & Woinowsky-Krieger (1970) for cylindrical elastic shells, and is still less accurate than theories 2 and 3. The last line of table 1 applies to the special case of isotropic ($m = \mathrm{d}/\mathrm{d}s = 0$) normal loading, for which the terms in the thin-sheet equations proportional to λ_1, λ_2, and λ_3 vanish identically by symmetry. Theories 1 to 4 are the same for this case, and predict both Ω and Δ to within relative errors of order ϵ^2. The errors appear in the high-curvature columns because κ is effectively of order unity for isotropic loading.

Most published theories for viscous sheets are special cases of the theory derived here. The simplest is that of Fliert *et al.* (1995), which neglects bending entirely; it corresponds to the last line of table 1. The 'viscida' theory of Buckmaster *et al.* (1975)

does include bending effects; but because it neglects the bending-induced stretching moment $N_2 = 5\mu H^3 K\Omega/6$, it corresponds to $\lambda_1 = 0$. Thus the accuracy of this theory will be that of either theory 3 or theory 4 in table 1, depending on the form assumed for the loading terms (Buckmaster *et al.* (1975) consider only the case $P^{\pm} = T^{\pm} = 0$). The theory of Howell (1996) is similar to that of Buckmaster *et al.* (1975) in neglecting the bending contribution to N.

6. Evolution of the sheet's geometry

Up to now, derivatives with respect to s have been written as total derivatives to emphasize that time plays no dynamical role in the thin-sheet equations. This is because the velocity of an inertialess sheet is determined entirely by its instantaneous geometry and the distribution of loads acting on it. However, in most situations of interest both the geometry and the loading will themselves change with time. Additional kinematic equations that describe the evolution of the sheet's shape, thickness, and length are therefore necessary. From now on, all derivatives with respect to s will be written as partial derivatives.

Let the shape of the midsurface be defined parameterically by an equation of the form

$$\boldsymbol{r}_0 = \boldsymbol{r}_0(s,t),$$

where s is arclength and t is time. Define the tangential component U and the normal component W of the 'midsurface velocity' as

$$U\boldsymbol{s} + W\boldsymbol{z} = \frac{\mathscr{D}\boldsymbol{r}_0}{\mathscr{D}t}, \tag{6.1}$$

where

$$\frac{\mathscr{D}}{\mathscr{D}t} = \frac{\partial}{\partial t} + u_e\frac{\partial}{\partial s}, \quad u_e = u_0(0,t) + \int_0^s \Delta_{\mathrm{mid}}\,\mathrm{d}s,$$

$u_0(0,t)$ is the rate at which new sheet material is supplied at $s = 0$ (e.g. from an extrusion slot), and Δ_{mid} is the rate of stretching of the midsurface. The operator $\mathscr{D}/\mathscr{D}t$ is a convective derivative that follows both the supply and stretching of the sheet, and was introduced (with $u_0(0,t) = 0$) by Buckmaster *et al.* (1975).

By differentiating (6.1) with respect to s and noting that $\partial\boldsymbol{r}_0/\partial s = \boldsymbol{s}$, $\partial\boldsymbol{s}/\partial s = K\boldsymbol{z}$, $\partial\boldsymbol{z}/\partial s = -K\boldsymbol{s}$, and $\mathscr{D}\boldsymbol{s}/\mathscr{D}t = \boldsymbol{z}\mathscr{D}\theta/\mathscr{D}t$, one obtains

$$\Delta_{\mathrm{mid}} = \frac{\partial U}{\partial s} - KW, \quad \frac{\mathscr{D}\theta}{\mathscr{D}t} = \frac{\partial W}{\partial s} + KU. \tag{6.2}$$

The next step begins with the kinematic conditions for the sheet's outer (material) surfaces $z = \pm H(s,t)/2$, which are (Fliert *et al.* 1995)

$$w_{\pm} - W = \pm\frac{1}{2}\frac{\partial H}{\partial t} \pm \frac{1}{2h_{\pm}}\left(u_{\pm} - U + u_e \pm \frac{H}{2}\frac{\partial\theta}{\partial t}\right)\frac{\partial H}{\partial s}, \tag{6.3}$$

where $u_{\pm}$ and $w_{\pm}$ are the fluid velocities at the outer surfaces. By combining the two ($\pm$) parts of (6.3), one obtains

$$h_+w_+ - h_-w_- = -KHW + \frac{\partial H}{\partial t} + \tfrac{1}{2}[u_+ + u_- - 2(U - u_e)]\frac{\partial H}{\partial s}. \tag{6.4}$$

By integrating the continuity equation (2.1a) across the sheet and using Leibniz's rule

for the derivative of a definite integral with variable limits, one obtains

$$h_+w_+ - h_-w_- = \tfrac{1}{2}(u_+ + u_-)\frac{\partial H}{\partial s} - \frac{\partial}{\partial s}\int_{-H/2}^{H/2} u\,\mathrm{d}z. \tag{6.5}$$

Equations (6.4) and (6.5) together imply

$$\frac{\mathscr{D}H}{\mathscr{D}t} = KHW + U\frac{\partial H}{\partial s} - \frac{\partial}{\partial s}\int_{-H/2}^{H/2} u\,\mathrm{d}z. \tag{6.6}$$

The exact evolution equations (6.2) and (6.6) can now be simplified further by exploiting the slenderness of the sheet. In the limit $\epsilon \to 0$, the midsurface is asymptotically close to a material surface, implying that the midsurface velocity (U, W) can be replaced by the fluid velocity (u_0, w_0) evaluated at the midsurface. This is most easily seen in the analytical solution (3.3) for an expanding annulus, for which $u_0 = U$ identically and $w_0 = W(1 - \epsilon^2/4)$, where $W = (w_+ + w_-)/2$. Second, referring to the decomposition (3.1) of the lateral velocity u, one sees that only the components $u_n\zeta^n$ with n even contribute to the integral in (6.6). However, the scaling analysis shows that u_0 exceeds u_2, u_4, etc. by factors of at least ϵ^{-2}, allowing one to set $u = u_0$ in the integral in (6.6). With these simplifications, the evolution equations become

$$\frac{\mathscr{D}\theta}{\mathscr{D}t} = \omega, \quad \frac{\mathscr{D}H}{\mathscr{D}t} = -H\Delta, \tag{6.7}$$

which are identical to those derived by Buckmaster *et al.* (1975) for the simpler case of uniform velocity across the sheet. Finally, the length $L(t)$ of the sheet satisfies

$$\frac{\partial L}{\partial t} = u_e(L, t). \tag{6.8}$$

7. Simple model problems

I turn now to some simple illustrative model problems. Viscous sheets respond to applied loads by some combination of bending and stretching, and a principal goal of this section will be to quantify the relative importance of these two modes of deformation. This can be done by calculating the rates of energy dissipation associated with each. Because the sheet is thin, the contribution of shear strains to the dissipation is negligible, and the dissipation rate per unit volume is, to lowest order,

$$4\mu e_{ss}^2 \sim 4\mu(\Delta + z\Omega)^2. \tag{7.1}$$

Integration of (7.1) across the sheet yields the dissipation rate Φ per unit area of the midsurface:

$$\Phi = \tfrac{1}{3}\mu H^3\Omega^2 + 4\mu H\Delta^2 \equiv \Phi_b + \Phi_s.$$

The dissipation is the sum of contributions due to bending (Φ_b) and stretching (Φ_s). The associated global dissipation rates for the sheet as a whole are

$$J_b(t) = \int_0^{L(t)} \Phi_b\,\mathrm{d}s, \quad J_s(t) = \int_0^{L(t)} \Phi_s\,\mathrm{d}s.$$

Finally, define the dissipation ratio

$$D(s,t) = \frac{\Phi_b}{\Phi_b + \Phi_s},$$

which represents the fraction of the local dissipation that is due to bending.

The dynamics of thin sheets will now be illustrated by three examples: inflation of a sheet by an excess pressure applied to one side ('film blowing'); deformation of a clamped 'viscous beam' under its own weight; and 'subduction' of a sheet extruded laterally in a gravitational field.

7.1. *Film blowing*

Consider an initially flat sheet of length L_0 and thickness $H_0 \equiv \epsilon L_0$ with fixed ends which is inflated by a constant excess pressure ΔP applied to one side. This is a simple prototype for more realistic models of bottle manufacture, and was studied by Fliert *et al.* (1995) using a simplified theory that neglected bending.

The equations governing the sheet's motion are

$$\frac{\mu}{3}\left[\frac{\partial^2}{\partial s^2} + \tfrac{5}{2}K^2\right](H^3\Omega) + 4\mu K H \Delta = \Delta P, \tag{7.2a}$$

$$\frac{\mu}{2}\left[K\frac{\partial}{\partial s} + \frac{5}{3}\frac{\partial K}{\partial s}\right](H^3\Omega) + 4\mu\frac{\partial}{\partial s}(H\Delta) = 0, \tag{7.2b}$$

together with the kinematic equations (6.7) and (6.8). The initial conditions are

$$H(s,0) - H_0 = \theta(s,0) = L(0) - L_0 = 0.$$

The boundary conditions depend how the ends $s = \pm L(t)/2$ of the sheet are attached to their supports. If the bending moments are zero there ('hinged' ends),

$$u_0(\pm L/2, t) = w_0(\pm L/2, t) = \Omega(\pm L/2, t) = 0. \tag{7.3}$$

If however the slope of the sheet at the ends is fixed ('clamped' ends),

$$u_0(\pm L/2, t) = w_0(\pm L/2, t) = \omega(\pm L/2, t) = 0.$$

The film evolves on two distinct time scales. Initially, it deforms purely by bending. Because the ends are fixed, however, stretching rapidly becomes important. The dissipation due to stretching becomes comparable to that due to bending after a time of order

$$\tau_b = \frac{\mu\epsilon^4}{\Delta P}, \tag{7.4}$$

the 'bending' time. Thereafter, the film deforms primarily by stretching on a slower time scale (Fliert *et al.* 1995)

$$\tau_s = \frac{\mu\epsilon}{\Delta P} \equiv \epsilon^{-3}\tau_b. \tag{7.5}$$

Non-dimensionalization of the governing equations using the length scale L_0, the time scale τ_b, and the velocity scale L_0/τ_b shows that the only dimensionless parameter in the problem is $\epsilon \equiv H_0/L_0$. For a given value of ϵ, the evolution of the sheet was determined numerically. At each time step, (7.2) were solved using the relaxation algorithm of Press *et al.* (1996). The sheet's geometry was then updated by solving the kinematic equations (6.7) using a second-order Runge–Kutta (midpoint) algorithm, treating the grid points as material points. The accuracy of the numerical code was tested against a small-time analytical solution.

Consider first the behaviour for short times $t \sim \tau_b$ after the pressure difference is applied. Figure 3 shows the total dissipation rates J_b and J_s due to bending and stretching, respectively, as functions of time for sheets with $\epsilon = 0.05$ and hinged ends (solid lines), $\epsilon = 0.05$ and clamped ends (dashed lines), and $\epsilon = 0.005$ and hinged ends (dotted lines). The intersection of the curves of J_b and J_s (solid, dashed, or dotted)

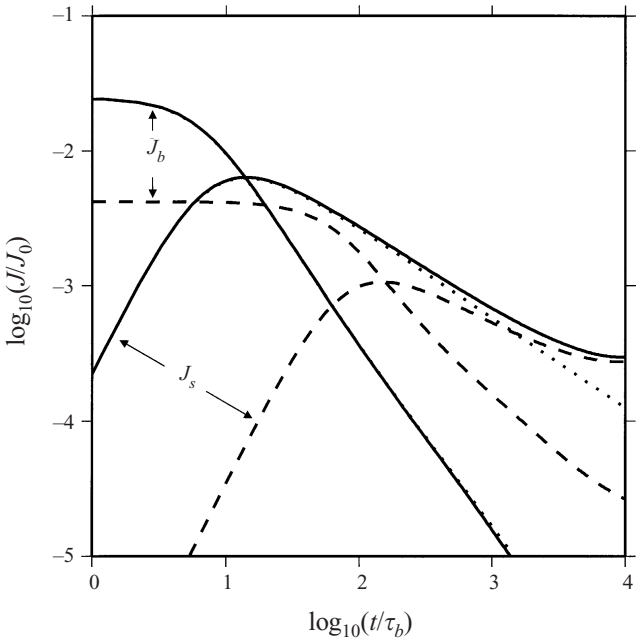

FIGURE 3. Total dissipation rates J_b and J_s due to bending and stretching, respectively, as functions of time for blown films with initial length L_0 and thickness $H_0 \equiv \epsilon L_0$. Solid lines: $\epsilon = 0.05$, hinged ends. Dashed lines: $\epsilon = 0.05$, clamped ends. Dotted lines: $\epsilon = 0.005$, hinged ends. Bending time scale τ_b is defined by (7.4), and $J_0 = \epsilon^3 \mu L_0^2/\tau_b^2$.

marks the time t_c of transition from bending- to stretching-dominated deformation. This transition occurs later for a clamped sheet ($t_c \sim 160\tau_b$) than for a hinged sheet ($t_c \sim 13\tau_b$). The reason can be seen in figure 4, which shows the local dissipation ratio D at various times for a sheet with $\epsilon = 0.005$ and either hinged (a) or clamped (b) ends. Only the portion $s \geqslant 0$ of the sheet is shown, and the fixed end is at the right. In both cases, $D = 1$ everywhere at $t = 0$ (except at isolated inflection points where $\Omega = \Delta = 0$). In the hinged sheet, D decreases uniformly everywhere, and is identically zero at the ends of the sheet where the bending moment vanishes by (7.3). In the clamped sheet, by contrast, D remains large in 'bending layers' near the ends of the sheet, whose width $\delta(t)$ can be determined by a simple scaling argument. In the boundary layer, the dominant terms in (7.2a) are the one on the right-hand side and the first on the left-hand side; their balance requires $\Omega \sim \Delta P \delta^2/\mu H^3$. Now the small-time analytical solution shows that $K \sim \epsilon t/L_0\tau_b$. This suggests that the curvature scales as ϵ divided by the characteristic length scale of the bending region, or $K \sim \epsilon/\delta$ in the boundary layer that eventually forms. The evolution equation $\mathrm{d}K/\mathrm{d}t \sim \Omega$ thus implies $\mathrm{d}\delta/\mathrm{d}t \sim L_0 \Delta P \delta^4/\mu H^4$, or

$$\delta \sim L_0 (t/\tau_b)^{-1/3}.$$

The correctness of this result is confirmed by the numerical solutions.

Consider now times $t \sim \tau_s$, when the film deforms mainly by stretching. Figure 5 shows the evolving shape of a film with $\epsilon = 0.05$ and either hinged (solid lines) or clamped ends (dashed lines). Only the half $x > 0$ of the film is shown. The evolution of the clamped film was not followed beyond $t \sim 2\tau_s$ because the bending

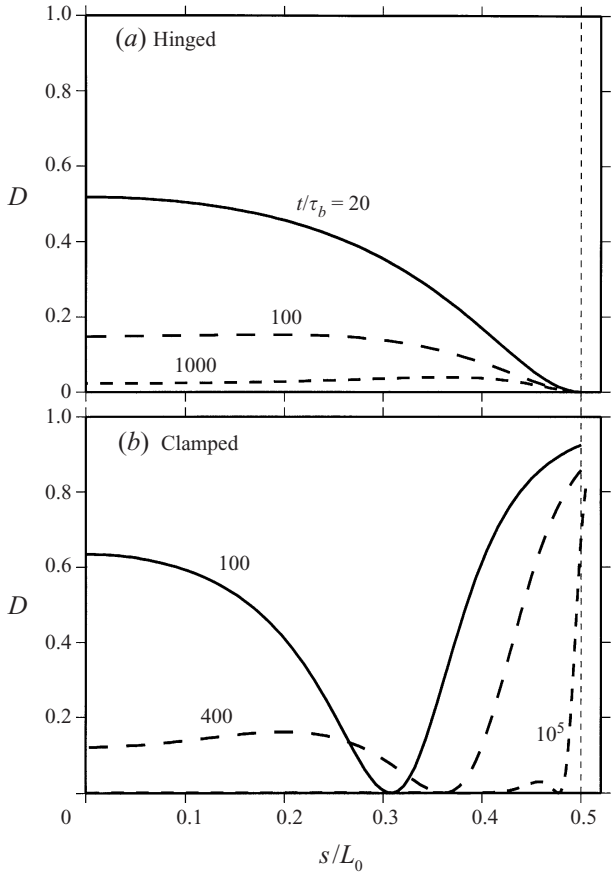

FIGURE 4. Local dissipation ratio D at various times for a blown film with $\epsilon = 0.005$ and either hinged (a) or clamped (b) ends. Only the portion $s \geqslant 0$ of the sheet is shown, and the fixed end is at the right. The curve for a clamped sheet at $t/\tau_b = 10^5$ extends beyond $s/L_0 = 0.5$ by an amount equal to the total stretching of the sheet up to that time. Bending time scale τ_b is defined by (7.4).

boundary layers become too thin to resolve numerically. When $t \sim \tau_s$, the hinged film describes a circular arc with a time-varying curvature $K(t)$ that is independent of ϵ, as predicted by the theory of Fliert *et al.* (1995). The effect of clamping the film is to modify its shape locally near the ends and to retard slightly its evolution relative to the hinged film. However, both of these effects become asymptotically small as $\epsilon \to 0$, and are already imperceptible at the scale of figure 5 when $\epsilon = 0.005$. Figure 6 shows the evolving lengths of the films whose shapes are displayed in figure 5. As far as one can tell from a numerical solution, the length goes to infinity after a finite time, in agreement with the prediction of Fliert *et al.* (1995). The same authors also showed that the blow-up time is sensitive to initial non-uniformities in the film thickness.

In summary, film blowing is dominated by stretching except initially ($t \sim \tau_b$) and in 'bending layers' of width $\delta \sim L_0(t/\tau_b)^{-1/3}$ at the clamped ends. In the limit $\epsilon \to 0$, therefore, bending is a singular perturbation of the stretching or 'membrane' dynamics of the film. The simplified theory of Fliert *et al.* (1995) is valid outside the initial and boundary layers, and predicts accurately the film's evolving length and shape.

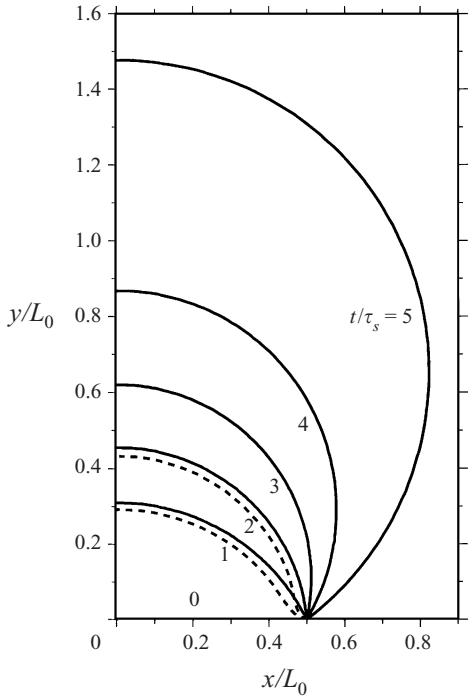

FIGURE 5. Shape of a blown film with $\epsilon = 0.05$ and either hinged (solid lines) or clamped (dashed lines) ends. Only half ($s > 0$) of the sheet is shown. Evolution of the clamped sheet was not followed beyond $t/\tau_s \sim 2$ because the bending boundary layers become too thin to resolve numerically. Stretching time scale τ_s is defined by (7.5).

7.2. *Viscous beam*

I now turn to a problem involving bending-dominated deformation: an initially horizontal 'viscous beam', clamped at one end and free at the other, which deforms under its own weight. This is the viscous analogue of the classic problem of an elastic beam, first treated by Galileo (1638). The equations governing the deformation are

$$\frac{\mu}{3}\left[\frac{\partial^2}{\partial s^2} + \tfrac{5}{2}K^2\right](H^3\Omega) + 4\mu K H \Delta = Hg\delta\rho\cos\theta, \tag{7.6a}$$

$$\frac{\mu}{2}\left[K\frac{\partial}{\partial s} + \frac{5}{3}\frac{\partial K}{\partial s}\right](H^3\Omega) + 4\mu\frac{\partial}{\partial s}(H\Delta) = Hg\delta\rho\sin\theta, \tag{7.6b}$$

together with the kinematic equations (6.7) and (6.8). Let the initial length and thickness of the beam be L_0 and $H_0 \equiv \epsilon L_0$, respectively. Then the initial conditions are

$$H(s,0) - H_0 = \theta(s,0) = L(0) - L_0 = 0$$

and the boundary conditions are

$$u_0(0,t) = w_0(0,t) = \omega(0,t) = \Delta(L,t) = \Omega(L,t) = \frac{\partial\Omega}{\partial s}(L,t) = 0. \tag{7.7}$$

The boundary conditions at $s = L$ are obtained by requiring the stress resultants and the bending moment to vanish there ($N = M = Q = 0$). The last condition in (7.7) is obtained from (2.4) (with $F_s^+ = F_s^- = 0$) by setting $Q = 0$ and neglecting the small

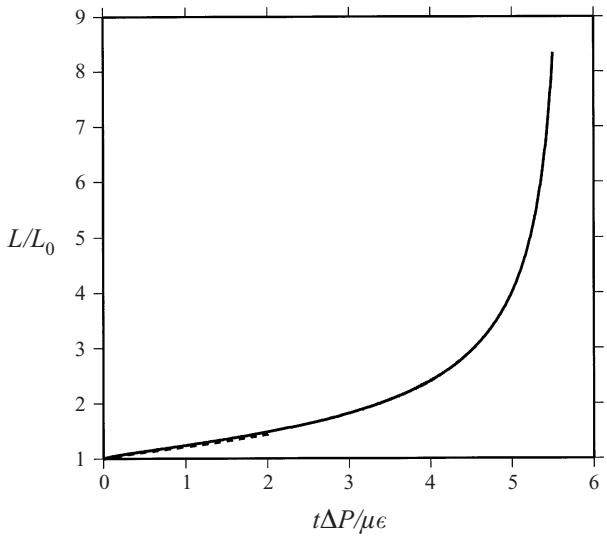

FIGURE 6. Length as a function of time of the blown films whose shapes are shown in figure 5.

term proportional to $\delta\rho$ (of order $\epsilon^2\,\mathrm{d}M/\mathrm{d}s$). Solutions of the above equations were obtained numerically using the same method as in the previous section, and tested against a small-time analytical solution.

Balancing the first term on the left-hand side of (7.6*a*) with the right-hand side and scaling the coordinate s by L_0 yields the characteristic velocity scale for the initial bending of the beam:

$$W_0 = \frac{g\delta\rho L_0^4}{\mu H_0^2}.$$

Equation (6.7) then yields the bending time scale

$$\tau_b = \frac{L_0}{W_0} \equiv \frac{\mu H_0^2}{g\delta\rho L_0^3}. \tag{7.8}$$

Figure 7 shows the shape of a beam with $\epsilon = 0.05$ as a function of t/τ_b. Curves for $\epsilon = 0.005$ are indistinguishable from those shown, except that the beam is slightly shorter at $t/\tau_b = 100$, having been stretched less. Because the beam has a finite resistance to (un-) bending, its lower part 'overshoots' the vertical between $t/\tau_b = 5$ and 10 before eventually returning to a near-vertical position.

Figure 8 shows the total dissipation rates $J_b(t)$ and $J_s(t)$ due to bending and stretching. Comparison of figures 7 and 8 shows that the sheet deforms primarily by bending until it is nearly vertical. The vertical part of the sheet then deforms further by stretching on a slower time scale

$$\tau_s \sim \frac{\mu}{L_0 g\delta\rho} \equiv \epsilon^{-2}\tau_b.$$

Bending is now confined to a boundary layer at the clamped end (visible as the rightward bulge near the top of the curve for $t/\tau_b = 100$).

7.3. *Extruded sheet*

In both engineering and geophysics, one often encounters thin viscous sheets that deform while being fed into a gravitational field. Thin sheets of polymer are often

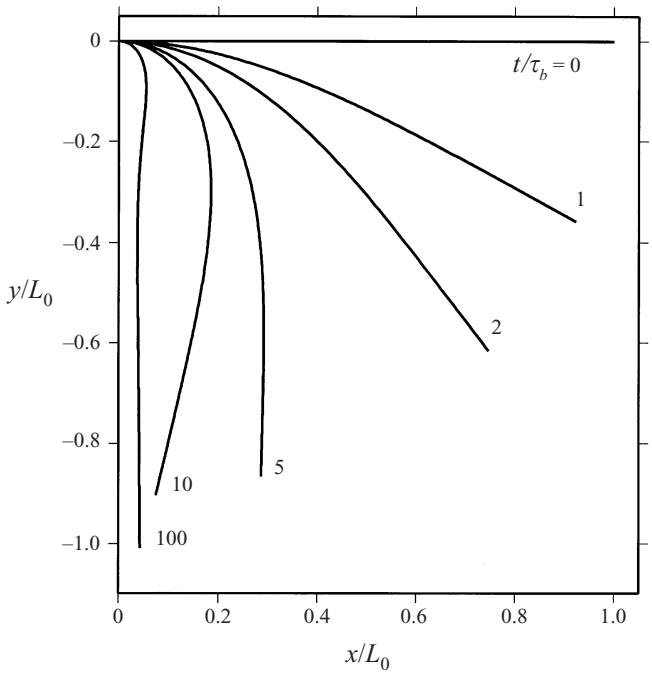

FIGURE 7. Deformation under gravity of an initially horizontal 'viscous beam' with its left end clamped and its right end free. The beam's initial length and thickness are L_0 and $H_0 = 0.05L_0$, respectively, and the bending time scale τ_b is defined by (7.8).

manufactured by extruding hot material from a narrow slit and letting it cool while it falls through air onto a rotating take-up roll (Pearson 1985). On the Earth, the oceanic lithosphere and skins on lava lakes move horizontally and cool, finally becoming dense enough to sink ('subduct') into the fluid below. Here I shall examine a simple model whose geometry resembles that of subduction: a viscous sheet fed horizontally at constant speed U_0 in a gravitational field. The quantity U_0 is thus analogous to what geophysicists call the 'plate speed'. An elastic analogue of this model, colourfully called the 'reverse spaghetti problem', was studied by Mansfield & Simmonds (1987).

I assume for simplicity that the stresses exerted on the sheet by the fluid around it are negligible. Then the governing equations and the boundary conditions at the sheet's leading end $s = L(t)$ are the same as for the viscous beam. However, the boundary conditions at the other end (the 'extrusion slit') $s = 0$ now become

$$u_0(0,t) - U_0 = w_0(0,t) = \omega(0,t) = 0.$$

Taking U_0 as the characteristic velocity scale and balancing the first term on the left-hand side of (7.6*a*) with the right-hand side, one obtains the characteristic length scale

$$L_1 = \left(\frac{\mu U_0 H_0^2}{g\delta\rho}\right)^{1/4}. \tag{7.9}$$

The time scale for bending is accordingly

$$\tau_b = \frac{L_1}{U_0} \equiv \left(\frac{\mu H_0^2}{U_0^3 g\delta\rho}\right)^{1/4}. \tag{7.10}$$

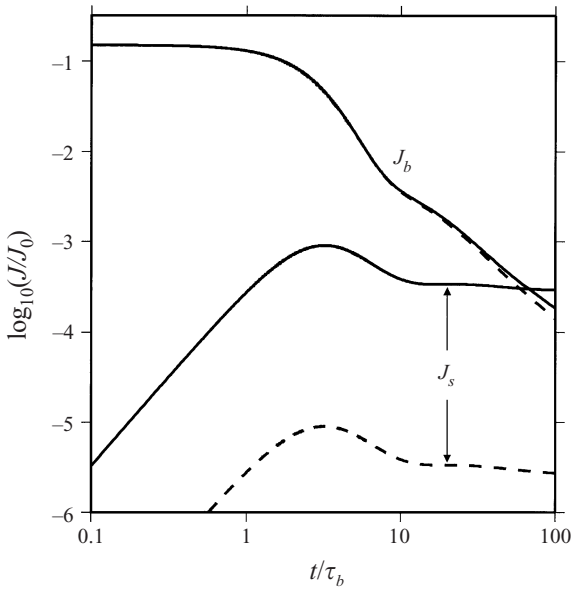

FIGURE 8. Total dissipation rates J_b and J_s due to bending and stretching, for a viscous beam with $\epsilon = 0.05$ (figure 7) (solid lines), and $\epsilon = 0.005$ (dashed lines). The bending time scale τ_b is defined by (7.8), and $J_0 = \epsilon^3 \mu L_0^2/\tau_b^2$.

Figure 9 shows the shape of an extruded sheet with $\epsilon \equiv H_0/L_1 = 0.05$ as a function of time. The numerical solution was started from a short horizontal 'proto-sheet' of length $0.1L_1$, and new material grid points were added as the length of the sheet increased. The evolution of a sheet with $\epsilon = 0.005$ is indistinguishable from that shown in figure 9. As for the viscous beam problem, the lower part of the sheet bends back on itself ($t/\tau_b = 3$) before becoming nearly vertical again ($t/\tau_b = 5$). Similar behaviour has been observed in finite-element modelling of subducted oceanic lithosphere (Houseman & Gubbins 1997). Unlike the viscous beam, however, the extruded sheet continues to deform primarily by bending. Figure 10 shows the bending and stretching dissipation rates J_b and J_s for sheets with $\epsilon = 0.05$ (solid lines) and $\epsilon = 0.005$ (dashed lines). For $t/\tau_b \leqslant 5$, J_b exceeds J_s by at least a factor of 100 (for $\epsilon = 0.05$) or 10 000 (for $\epsilon = 0.005$). This is because the new undeformed sheet material that is continuously being extruded horizontally must bend before it can fall vertically.

Before applying this simple model to subduction one must verify that the length and time scales involved make sense. A typical velocity of plate convergence at subduction zones around the Pacific Ocean is about 8 cm yr^{-1}, or $2.5 \times 10^{-9}\,\mathrm{m\,s}^{-1}$ (Garfunkel, Anderson & Schubert 1986, table 1). Assuming further $H_0 = 100$ km, $10^{25} \leqslant \mu \leqslant 10^{26}$ Pa s, $g = 9.8\,\mathrm{m\,s}^{-2}$, and $\delta\rho = 70\,\mathrm{kg\,m}^{-3}$, one finds from (7.9) that $800 \leqslant L_1 \sim 1400$ km. These values are of the same order as the depths of the Earth's upper mantle (700 km) and whole mantle (2900 km). They also imply that $L_1 \gg H_0$, which is required for the thin-sheet approximation to be valid. The associated time scale is $10 \leqslant \tau_b \leqslant 18$ Ma.

The evolution of an extruded sheet provides a simple explanation for the phenomenon of 'trench rollback' in global plate tectonics. It has long been known that the subducted portion of an oceanic plate does not just descend parallel to its dip, but also moves transverse to it, in the direction opposite to the velocity of the surface

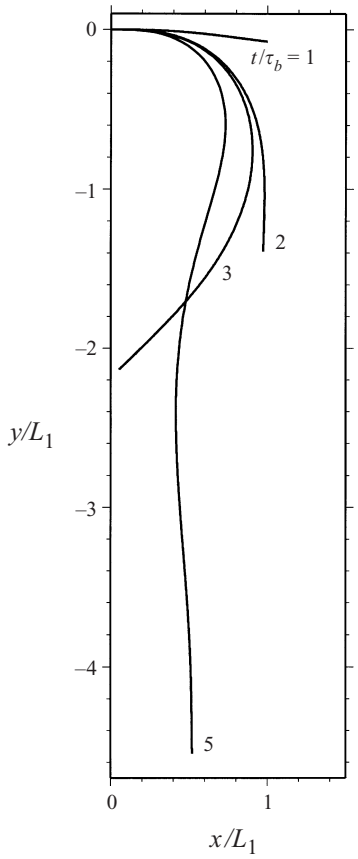

FIGURE 9. Evolving shape of a sheet with $\epsilon \equiv H_0/L_1 = 0.05$ extruded horizontally in a gravitational field. Length scale L_1 is defined by (7.9), and time scale τ_b by (7.10).

portion. This causes the 'hinge point' between the subducted and surface portions to migrate with a velocity $U_{rb} < 0$, i.e. in the direction opposite to the surface plate velocity (Elsasser 1971). Garfunkel *et al.* (1986) suggested that such retrograde motion is caused by the bending of the plate due to the pull exerted by its sinking subducted portion, but their kinematic model did not include bending explicitly. Subsequent models (Griffiths, Hackney & van der Hilst 1995; Guillou-Frottier, Buttles & Olson 1995; Christensen 1996) have generally specified the velocity of retrograde motion *a priori* rather than attempting to determine it dynamically.

The present model permits such a determination. Let the location of subduction (the 'trench') be defined as the point where the dip of the sheet attains a specified value θ_0. Figure 11 shows the velocity U_{rb} of this point as a function of time, for $\theta_0 = 5°$; curves of similar shape obtain for other choices of θ_0. The dip θ_0 is first reached by the leading end of the sheet at $t \sim 0.95\tau_b$. The rollback speed initially greatly exceeds the plate speed, but then quickly decreases. Throughout the stage of 'mature' subduction (corresponding to a penetration depth of a few hundred km, or roughly $1.2 \leqslant t/\tau_b \leqslant 2.0$), $|U_{rb}| \leqslant U_0$. This agrees with estimates for subduction zones on Earth, for which $0 \leqslant U_{rb}/U_0 \leqslant 0.9$ (Garfunkel *et al.* 1986, tables 1 and 2). It should be noted, however, that the decrease of U_{rb} with time is partly a consequence of the fixed extrusion slit in the model, which prevents the hinge point from moving beyond it.

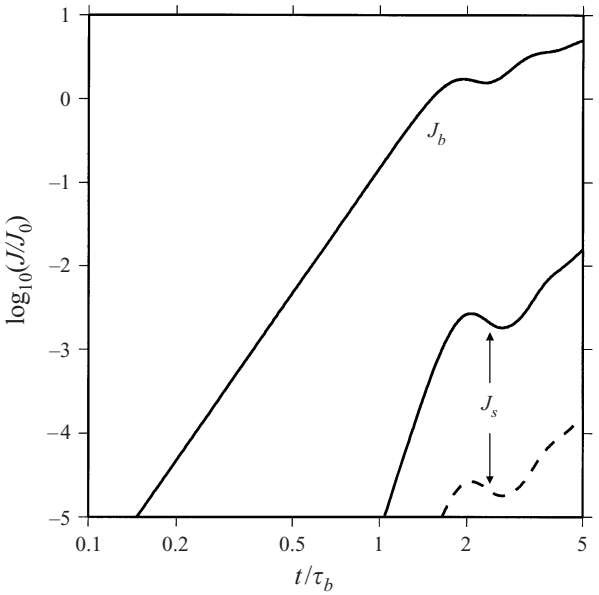

FIGURE 10. Total dissipation rates J_b and J_s due to bending and stretching for horizontally extruded sheets with $\epsilon = 0.05$ (solid lines) and $\epsilon = 0.005$ (dashed lines). Solid and dashed lines for bending coincide.

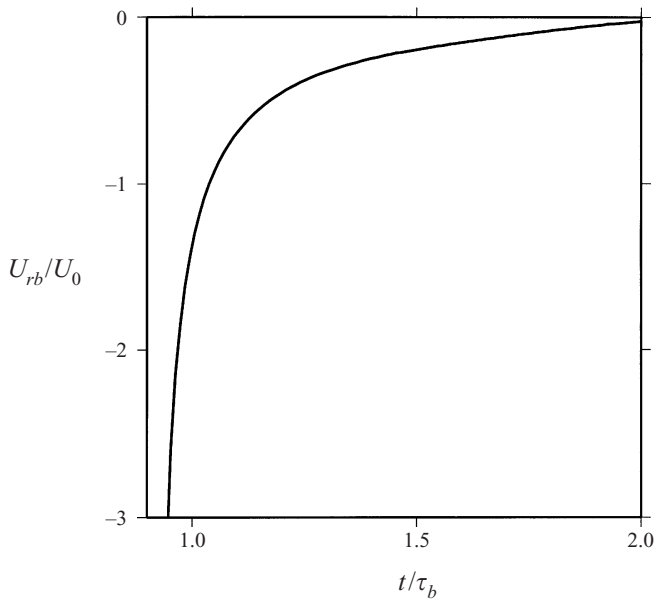

FIGURE 11. Normalized rollback speed U_{rb}/U_0 as a function of time for the sheet shown in figure 9. Definition of U_{rb} is discussed in the text.

The model just presented is highly idealized, and should not be overinterpreted. On Earth, the velocity U_0 is not externally specified, but is itself determined by the dynamics of the sinking plate. Other important factors neglected in the model include the resistance of the ambient fluid, the stress- and temperature-dependence of mantle rheology, and the intrinsic three-dimensionality of most subduction zones.

Consideration of these is beyond the scope of this study, whose modest goal is to quantify just one aspect of subduction dynamics.

8. Discussion

In this study, equations have been derived that describe the response of a viscous sheet of any shape to arbitrary loading. The only requirements are that the sheet's thickness be small relative to the characteristic lateral scale L of the deformation ($\epsilon \ll 1$), and that its radius of curvature not be much smaller than L ($\kappa = O(1)$). Because the sheet can respond to loading either by stretching or by bending, it was necessary to perform separate asymptotic expansions for these two regimes, and then to combine the results into uniformly valid composite expressions for the moments N and M. The final equations thus contain both stretching and bending terms, which correspond respectively to the 'outer' and 'inner' (boundary layer) expansions of matched asymptotics. The correctness of the equations was checked against analytical solutions for a loaded cylindrical annulus.

Of course the thin-sheet equations derived here become invalid whenever the underlying assumption of slenderness is violated. This will occur in regions of width $\sim H$ near the sheet's boundaries, and also at points where the sheet's radius of curvature is too small ($K^{-1} \sim H$). However, the equations remain valid in bending bounding layers as long as their thickness $\delta \gg H$, and *a fortiori* in portions of the sheet dominated by stretching.

The equations derived here contain several new terms, including the bending-induced stretching moment $N_2 = 5\mu H^3 K \Omega/6$ and the non-local inhomogeneous terms in (4.11). The error analysis for bending-dominated deformations (table 1, theories 1–4) shows that neglecting these terms degrades the accuracy of the solutions of the thin-sheet equations, giving rise to relative errors of order unity in some cases. The most serious of these is the error in u_0, w_0 and Ω for tangential loading at low curvature ($\kappa \sim \epsilon$), which results from neglecting the non-local tangential load term in (4.11*a*). The errors of order unity in the stretching rate Δ which result from neglecting N_2 are less serious because stretching makes a relatively small contribution to the total dissipation rate in these bending-dominated deformations.

The intrinsic coupling between bending and stretching of thin sheets becomes clearer if the composite expansions (4.10) are written in matrix form, neglecting for clarity the inhomogeneous terms:

$$\begin{pmatrix} N \\ M \end{pmatrix} = \begin{pmatrix} 4\mu H & 5\mu H^3 K/6 \\ \mu H^3 K/3 & \mu H^3/3 \end{pmatrix} \begin{pmatrix} \Delta \\ \Omega \end{pmatrix}.$$

The 2×2 matrix above is a coupling matrix between the moments N and M and the rates of stretching (Δ) and bending (Ω). Its diagonal elements measure the effects of pure stretching and bending, i.e. the stretching moment induced by stretching and the bending moment induced by bending. The off-diagonal elements are mixed terms that represent the stretching moment induced by bending (upper right) and the bending moment induced by stretching (lower left). Both off-diagonal elements are proportional to K, showing that the sheet's curvature is the factor responsible for the coupling.

Because the thin-sheet equations derived here include both stretching and bending effects, the partitioning of the deformation between the two modes is automatically determined as part of the solution. This partitioning depends on three factors: the geometry of the sheet, the distribution of loads acting on it, and the boundary

conditions. In all three model problems treated here (film blowing, viscous beam, extruded sheet), the geometry is such that the loading is purely normal at $t = 0$. The sheet therefore deforms initially by pure bending with insignificant stretching, regardless of the boundary conditions. The subsequent evolution, however, depends critically on these conditions. In the film blowing problem, the ends of the sheet are fixed. The sheet therefore has no choice but to evolve by stretching, even though the loading remains purely normal. Indeed, the constraint of fixed ends is so strong that the initial bending lasts only for an 'instant' of order ϵ^3 times the sheet's blow-up time. Bending remains important in thin boundary layers near clamped ends, where the boundary conditions are incompatible with pure stretching, but the thickness of these layers decreases rapidly on the same short time scale.

The viscous beam, by contrast, has one clamped end and one free end. Deformation therefore takes place principally by bending until most of the sheet is vertical. This part of the sheet now has small curvature and is loaded tangentially, and thus deforms primarily by stretching, but on a much slower time scale. Bending remains important only in a boundary layer near the clamped end whose thickness decreases with time. The behaviour of a viscous beam is in a sense opposite to that of a blown film: the deformation is almost entirely by bending during the period of its greatest intensity, as measured by the dissipation rate (figure 8). Bending is even more dominant in an extruded sheet (figure 10), where the bending boundary layer is thickened by the continual advection of undeformed sheet material from the extrusion slit.

Evidently the next step is to extend the theory presented here to three-dimensional and axisymmetric sheets having two (generally distinct) principal curvatures K_1, K_2 at each point. The theory of three-dimensional elastic shells (e.g. Novozhilov 1959; Calladine 1983) suggests that the partitioning of the deformation between stretching and bending will depend in a complicated way on the interaction of the sheet's geometry with the distribution of the applied loading. Further progress on this difficult problem will require another study.

This research was supported by the United States National Science Foundation grant 97-07604. I thank V. Barcilon, C. Calladine, A. Davaille, M. Loewenberg, E. Onat, E. Sanchez-Palencia, and J. Simmonds for helpful discussions, and P. Howell and two anonymous referees for thorough and constructive reviews. Algebraic manipulations were performed using Mathematica 3.0 (Wolfram 1996).

Appendix. Analytical solutions for a loaded cylindrical annulus

The geometry of the model is sketched in figure 2. Expressions are given below in the limit $\epsilon \equiv mH/R \ll 1$ for the velocity components u_0 and w_0 at the midsurface, the stress resultant (stretching moment) N, and the bending moment M, for both normal ($P \neq 0$, $T = 0$) and tangential ($T \neq 0$, $P = 0$) loading. In each expansion, terms of order ϵ^4 times the leading term and smaller are neglected, and $\chi = m^2 - 1$.

A.1. *Normal loading*

$$u_0 = -\frac{3PLm^3}{\epsilon^3\mu\chi^2}\left(1 + \frac{\epsilon}{2m} + \frac{4m^2-1}{20m^2}\epsilon^2 + \frac{2+2m^2+5m^4}{120m^3}\epsilon^3\right)\sin m\phi,$$

$$w_0 = \frac{3PLm^4}{\epsilon^3\mu\chi^2}\left(1 + \frac{\epsilon}{2m} + \frac{13m^2-7}{40m^2}\epsilon^2 + \frac{13m^2-7}{80m^3}\epsilon^3\right)\cos m\phi,$$

$$N = -\frac{PLm}{\chi}\left(1 + \frac{\epsilon}{2m} - \frac{\epsilon^3}{40m}\right)\cos m\phi,$$

$$M = \frac{PL^2m^2}{\chi}\left(1 + \frac{\epsilon}{2m}\right)\cos m\phi.$$

A.2. *Tangential loading*

$$u_0 = \frac{3TLm^2}{\epsilon^3\mu\chi^2}\left(1 - \frac{m^2-2}{2m}\epsilon + \frac{17-13m^2+5m^4}{60m^2}\epsilon^2 + \frac{4-8m^2+13m^4}{120m^3}\epsilon^3\right)\sin m\phi,$$

$$w_0 = -\frac{3TLm^3}{\epsilon^3\mu\chi^2}\left(1 - \frac{m^2-2}{2m}\epsilon + 3\frac{m^2+1}{40m^2}\epsilon^2 - \frac{14-23m^2+3m^4}{80m^3}\epsilon^3\right)\cos m\phi,$$

$$N = \frac{TLm^2}{\chi}\left(1 + \frac{\epsilon}{2m} + \frac{m^2-2}{40m^3}\epsilon^3\right)\cos m\phi,$$

$$M = -\frac{TL^2m}{\chi}\left(1 - \frac{m^2-2}{2m}\epsilon - \frac{m^2-1}{4m^2}\epsilon^2\right)\cos m\phi.$$

REFERENCES

Buckmaster, J. D., Nachman, A. & Ting, L. 1975 The buckling and stretching of a viscida. *J. Fluid Mech.* **69**, 1–20.

Calladine, C. R. 1983 *Theory of Shell Structures*. Cambridge University Press.

Christensen, U. R. 1996 The influence of trench migration on slab penetration into the lower mantle. *Earth Planet. Sci. Lett.* **140**, 27–39.

Ciarlet, P. G. 1998 *Introduction to Linear Shell Theory*. Gauthier-Villars.

Ellis, S., Fullsack, P. & Beaumont, C. 1995 Oblique convergence of the crust driven by basal forcing: implications for length-scales of deformation and strain partitioning in orogens. *Geophys. J. Intl* **120**, 24–44.

Elsasser, W. 1971 Sea floor spreading and thermal convection. *J. Geophys. Res.* **76**, 1101–1111.

England, P. & McKenzie, D. 1982 A thin viscous sheet model for continental deformation. *Geophys. J. R. Astr. Soc.* **70**, 295–321.

England, P. & McKenzie, D. 1983 Correction to: a thin viscous sheet model for continental deformation. *Geophys. J. R. Astr. Soc.* **73**, 523–532.

Fliert, B. W. van de, Howell, P. D. & Ockenden, J. R. 1995 Pressure-driven flow of a thin viscous sheet. *J. Fluid Mech.* **292**, 359–376.

Galileo, G. 1638 *Discorsi e Dimostrazioni Matematiche Intorno à due Nuove Scienze*. Leiden.

Garfunkel, Z., Anderson, C. A. & Schubert, G. 1986 Mantle circulation and the lateral migration of subducted slabs. *J. Geophys. Res.* **91**, 7205–7223.

Goldenveizer, A. L. 1961 *Theory of Elastic Thin Shells*. Pergamon.

Goldenveizer, A. L. 1963 Derivation of an approximate theory of shells by means of asymptotic integration of the equations of the theory of elasticity. *Prikl. Mat. Mech.* **27**, 593–608.

Green, A. E. & Zerna, W. 1992 *Theoretical Elasticity*. Dover.

Griffiths, R. W., Hackney, R. I. & Hilst, R. van der 1995 A laboratory investigation of effects of trench migration on the descent of subducted slabs. *Earth Planet. Sci. Lett.* **133**, 1–18.

Guillou-Frottier, L., Buttles, J. & Olson, P. 1995 Laboratory experiments on the structure of subducted lithosphere. *Earth Planet. Sci. Lett.* **133**, 19–34.

Houseman, G. A. & Gubbins, D. 1997 Deformation of subducted oceanic lithosphere. *Geophys. J. Intl* **131**, 535–551.

Howell, P. D. 1996 Models for thin viscous sheets. *Eur. J. Appl. Math.* **7**, 321–343.

Love, A. E. H. 1944 *A Treatise on the Mathematical Theory of Elasticity*, 4th Edn. Dover.

Mansfield, L. & Simmonds, J. G. 1987 The reverse spaghetti problem: drooping motion of an elastica issuing from a horizontal guide. *Trans. ASME: J. Appl. Mech.* **54**, 147–150.

Medvedev, S. E. & Podladchikov, Y. Y. 1999 New extended thin-sheet approximation for geodynamic applications – I. Model formulation. *Geophys. J. Intl* **136**, 567–585.

Niordson, F. I. 1985 *Shell Theory*. North-Holland.

Novozhilov, V. V. 1959 *The Theory of Thin Shells*. P. Noordhoff.

Pearson, J. R. A. & Petrie, C. J. S. 1970*a* The flow of a tubular film. Part 1. Formal mathematical representation. *J. Fluid Mech.* **40**, 1–19.

Pearson, J. R. A. & Petrie, C. J. S. 1970*b* The flow of a tubular film. Part 2. Interpretation of the model and discussion of solutions. *J. Fluid Mech.* **42**, 609–625.

Pearson, J. R. A. 1985 *Mechanics of Polymer Processing*. Elsevier.

Press, W. H., Teukolsky, S. A., Vetterling, W. T. & Flannery, B. P. 1996 *Numerical Recipes in Fortran 77: The Art of Scientific Computing*, 2nd Edn. Cambridge University Press.

Ribe, N. M. 1992 The dynamics of thin shells with variable viscosity and the origin of toroidal flow in the mantle. *Geophys. J. Intl* **110**, 537–552.

Sanchez-Palencia, E. 1990 Passages à la limite de l'élasticité tri-dimensionnelle à la théorie asymptotique des coques minces. *C. R. Acad. Sci. Paris* I **309**, 909–916.

Timoshenko, S. P. & Woinowsky-Krieger, S. 1970 *Theory of Plates and Shells*, 2nd Edn. McGraw-Hill.

Weinstein, S. A. & Olson, P. 1992 Thermal convection with non-Newtonian plates. *Geophys. J. Intl* **111**, 515–530.

Wolfram, S. 1996 *The Mathematica Book*, 3rd Edn. Wolfram Media/Cambridge University Press.